Variations of Retinal Nerve Fiber Layer Thickness and Ganglion Cell–Inner Plexiform Layer Thickness According to the Torsion Direction of Optic Disc

Kang Hoon Lee,[1] Chan Yun Kim,[2] and Na Rae Kim[1]

[1]Department of Ophthalmology and Inha Vision Science Laboratory, Inha University School of Medicine, Incheon, Korea
[2]Institute of Vision Research, Department of Ophthalmology, Yonsei University College of Medicine, Seoul, Korea

Correspondence: Na Rae Kim, Department of Ophthalmology, Inha University Hospital, 7-206, 3-ga, Shinheung-dong, Jung-gu, Incheon, 400-711, Korea; nrkim@inha.ac.kr.

Submitted: May 9, 2013
Accepted: January 12, 2014

Citation: Lee KH, Kim CY, Kim NR. Variations of retinal nerve fiber layer thickness and ganglion cell–inner plexiform layer thickness according to the torsion direction of optic disc. *Invest Ophthalmol Vis Sci.* 2014;55:1048–1055. DOI:10.1167/iovs.13-12380

Purpose. To examine the relationship between the optic disc torsion and peripapillary retinal nerve fiber layer (RNFL) thickness through a comparison with the macular ganglion cell inner plexiform layer complex (GCIPL) thickness measured by Cirrus optical coherence tomography (OCT).

Methods. Ninety-four eyes of 94 subjects with optic disc torsion and 114 eyes of 114 subjects without optic disc torsion were enrolled prospectively. The participants underwent fundus photography and OCT imaging in peripapillary RNFL mode and macular GCIPL mode. The participants were divided into groups according to the presence or absence of optic disc torsion. The eyes with optic disc torsion were further divided into supranasal torsion and inferotemporal torsion groups according to the direction of optic disc torsion. The mean RNFL and GCIPL thicknesses for the quadrants and subsectors were compared. The superior and inferior peak locations of the RNFL were also measured according to the torsion direction.

Results. The temporal RNFL thickness was significantly thicker in inferotemporal torsion, whereas the GCIPL thickness at all segments was unaffected. The inferotemporal optic torsion had more temporally positioned superior peak locations of the RNFL than the nontorsion and supranasal-torted optic disc.

Conclusions. Thickening of the temporal RNFL with a temporal shift in the superior peak within the eyes with inferotemporal optic disc torsion can lead to interpretation errors. The ganglion cell analysis algorithm can assist in differentiating eyes with optic disc torsion.

Keywords: optical coherence tomography, ganglion cell–inner plexiform layer, retinal nerve fiber layer, optic disc torsion

Optic disc torsion is a relatively frequent finding during the course of a routine ophthalmic examination, which represents the skewed insertion of the optic nerve into the globe. This condition has been suggested to have embryologic origins.[1–4] Traditionally, some studies regard optic disc torsion as one of the major components of tilted disc syndrome, which has been classically considered to include the following signs: optic disc torsion, optic disc dysversion, situs inversus of the retinal vessels, beta-peripapillary atrophy, inferonasal chorioretinal thinning, posterior staphyloma, or coloboma, and manifests as various types of visual field defects.[1–5] On the other hand, there is no consensus on the definition of a tilted optic disc and optic disc torsion. Therefore, a diagnosis is often made in the absence of objectively derived criteria, which often creates confusion when attempting to distinguish between a tilted optic disc and optic disc torsion.

Two major geometric relationships exist between the optic nerve head and its point of entry through the sclera. Normal optic discs are minimally oval with a slightly longer vertical diameter than the horizontal shape, and the sagittal axis of the optic disc is almost perpendicular to the horizontal line connecting the fovea.[6] As a definition of the tilted optic disc, the amount of tilt is normally estimated by disc "ovality," which is measured by the ratio between the longest and shortest diameters of the optic disc (index of tilt = shortest diameter/longest diameter).[7–12] The optic disc is classified as a tilted disc when the index of the tilt is more than 0.75. The second geometric variable in optic discs is a rotation about the sagittal axis of the optic nerve. This variable is referred to in the literature as optic disc torsion. Optic disc torsion can be viewed and measured in two-dimensional space. The longest diameter normally falls within 15° of the vertical meridian. Torted, by definition, is defined as 15° beyond the axis means.[5,12,13] The vast majority of reports, however, do not make a distinction between optic disc tilt and the tilt and torsional components of the anomaly.

In recent years, spectral-domain optical coherence topography (OCT) enables more detailed and precise quantitative assessments of glaucomatous structural changes, and the use of algorithms for intraretinal segmentation allows separate assessments of individual retinal layers rather than assessments of total retinal thickness.[14,15] Furthermore, OCT enables retinal ganglion cell layer thickness of the human macula to be measured in vivo. Recent studies conducted using the Cirrus HD-OCT (Carl Zeiss Meditec, Dublin, CA) have reported that the ganglion cell analysis (GCA) algorithm can detect and

measure the thickness of the macular ganglion cell–inner plexiform layer (GCIPL) with excellent intervisit reproducibility and with a diagnostic power that is comparable to conventional peripapillary retinal nerve fiber layer (RNFL) measurements.[16–19] This report focused on the optic disc torsion itself, with or without optic disc tilt. The present study examined the association between optic disc torsion and the distribution of the retinal ganglion cell, RNFL measured by the macular GCIPL, and circumpapillary RNFL parameters using Cirrus HD-OCT.

Materials and Methods

Subjects

This was a prospective comparative study of healthy subjects with or without optic disc torsion. A total of 208 consecutive subjects, who were examined by a single glaucoma specialist (NRK) from March 2012 to September 2013 at the glaucoma clinic of the Inha University Hospital, Incheon, Korea, were enrolled in this study. Before initiating the study, the subjects provided written informed consent for study participation. The study was performed in accordance with the ethical standards of the Declaration of Helsinki, and was approved by the institutional review board of Inha University Hospital.

A total of 94 subjects with optic disc torsion were enrolled in this study, and their data were compared with those of 114 subjects without optic disc torsion. For both subjects with and without optic disc torsion, the eligibility was determined by a complete ophthalmologic examination, including a review of the medical history, measurements of the best-corrected visual acuity, Goldmann applanation tonometry, manifestation refraction, slit-lamp examination of the anterior segment, gonioscopy, dilated fundus examination, red-free fundus photography (Canon, Tokyo, Japan), visual field testing with Humphrey standard automated perimetry (Carl Zeiss Meditec), and Cirrus OCT. The central corneal thickness, anterior chamber depth, and axial length in each patient were also measured during the initial presentation using ultrasound pachymetry (Tomey Corporation, Nagoya, Japan) and contact A-scan ultrasound biometry (Storz Omega Compu-Scan Biometric Ruler; Storz International, St. Louis, MO).

All patients met the following inclusion criteria to be entered into the study: a consistent best corrected visual acuity of 20/30 or better with a refractive error between +4.00 and −6.00 diopters (D), IOP of 21 mm Hg or lower, open angle on gonioscopy, reliable visual fields (a mean deviation or a pattern SD within the 95% confidence interval, defined as false negative $< 15\%$, false-positive $< 15\%$, and fixation losses $< 20\%$), and no evidence of glaucomatous defects on a visual field examination. Patients were excluded based on the following criteria: a history of retinal disease, including diabetic or hypertensive retinopathy, high myopia exceeding −6.00 D of spherical equivalent refractive error, history of eye trauma or surgery including a laser treatment and uncomplicated cataract surgery, other optic nerve disease including glaucoma, and history of systemic or neurological diseases that can affect the visual field. The exclusion of glaucoma was based on the red-free fundus photography–localized or diffuse RNFL defect or glaucomatous optic disc changes (such as diffuse or localized rim thinning, disc hemorrhage, a notch in the rim, and a vertical cup-to-disc ratio higher than that of the other eye by more than 0.2). If both eyes of a patient met the inclusion criteria, one eye was chosen randomly for the study.

Measurement of the Optic Disc Tilt and Torsion

After cycloplegia, digital retinal photographs centered on the optic disc and macula were obtained using standardized settings with a nonmydriatic retinal camera (Canon CR6-45NM retinal camera, EOS-D60 digital camera; Canon). The optic disc tilt and torsion were measured from these photographs on a liquid crystal display monitor by two independent observers (KHL, NRK) using the National Institutes of Health image analysis software (Image J software version 1.45; available at http://rsb.info.nih.gov/ij/index.html; developed by Wayne Rasband; National Institutes of Health, Bethesda, MD). To evaluate the interobserver reproducibility of the measurements of the index of tilt and torsion degree, 30 randomly selected disc photographs were evaluated by two examiners.

Optic disc tilting was diagnosed when one margin of the optic disc was raised above the opposite margin, as observed from the stereoscopic photographs using a stereoscopic viewer. The halo surrounding the optic disc was identified but not included in the measurements. Optic disc tilt was identified by the tilt ratio, which is defined as the ratio between the longest and shortest diameters of the optic disc (index of tilt = shortest diameter/longest diameter). When the index of tilt was more than 0.75, the optic disc was classified as a tilted disc.[5,8–10]

Optic disc torsion was identified and defined as a deviation of the long axis of the optic disc from the vertical meridian. The vertical meridian was identified as a vertical line 90° from a horizontal line connecting the fovea, which is 2° to 6° below the optic disc, to the center of the optic disc; that is, different from horizontal raphe. The optic disc was classified as optic disc torsion when the degree of torsion was more than 15°. A positive torsion value indicated supranasal torsion, and a negative value indicated inferotemporal torsion. On the other hand, the state of optic disc nontorsion was defined as a torsion degree of less than 15°.[5,8–10,13]

Optical Coherence Tomography Imaging

A Cirrus HD-OCT (version 6.0 software) was used to acquire one macular (Macular Cube 514 × 128 protocol) and one optic disc (Optic Disc Cube 200 × 200 protocol) scan in each qualifying eye. The macular cube protocol included macula thickness analysis and GCA. The Optic Disc Cube protocol included optic nerve head (ONH) and RNFL analysis. Only good-quality scans were used for the analysis. Good quality was defined as scans with a signal strength of 6 or more, without RNFL discontinuity or misalignment, involuntary saccade, or blinking artifacts and an absence of algorithm segmentation failure on a careful visual inspection.

The GCA algorithm detects and measures the thickness of the macular GCIPL within a 14.13 mm^2 elliptical annulus area centered on the fovea. Processing was performed in three dimensions. The following GCIPL thickness measurements were analyzed: mean, minimum, and sectoral (superior, superonasal, inferonasal, inferior, inferotemporal, and superotemporal). The parameters from the retinal thickness included the central subfield thickness, cube volume, and cube average thickness. These were also measured automatically using the Cirrus internal macular thickness analysis algorithm.

The following RNFL thickness measurements were analyzed: mean and sectoral (temporal, superior, nasal, and inferior). The parameters from ONH analysis included the rim area, optic disc area, mean cup-to-disc area ratio, vertical cup-to-disc diameter ratio, and cup volume, which were measured automatically using the Cirrus internal ONH analysis algorithm.

Table 1. Characteristics of the Subjects According to the Presence of Disc Torsion

Characteristics	Optic Disc Torsion, $n = 94$	Optic Disc Nontorsion, $n = 114$	P Value‡
Age, y	48.29 ± 13.64	50.59 ± 13.02	0.216
Female, *n*, %*	46, 48.9	45, 39.5	0.171
Spherical equivalent error, D	−1.02 ± 1.95	−0.96 ± 1.95	0.841
Axial length, mm	23.87 ± 1.02	23.09 ± 4.05	0.346
Anterior chamber depth, mm	3.08 ± 0.49	3.12 ± 0.40	0.714
Torsion degree†	33.32 ± 18.61	7.32 ± 3.98	<0.001
Index of tilt	0.88 ± 0.07	0.88 ± 0.07	0.596
Tilted disc, %*	5, 5.3	4, 3.5	0.734
Situs inversus, %*	39, 41.5	14, 12.3	<0.001
Beta-peripapillary atrophy, %*	29, 30.9	31, 27.2	0.562
Mean IOP, mm Hg	14.00 ± 2.86	14.63 ± 3.28	0.153
Central corneal thickness, μm	544.91 ± 34.81	555.79 ± 38.62	0.234
Mean deviation, dB	−1.30 ± 1.69	−1.40 ± 1.69	0.720
Pattern standard deviation, dB	2.03 ± 1.33	1.73 ± 0.74	0.090

Data are given as mean ± SD.
* Nonparametric values were compared by chi-square test.
† An absolute value was used in this analysis.
‡ Value for comparing optic disc torsion and optic disc nontorsion.

Definition and Measurement of Angle Alpha and Angle Beta by Optical Coherence Tomography Imaging

Superior and inferior peak locations were calculated according to the method described in a previous study. In previous studies, Hwang et al.[20,21] introduced a method to determine the peak locations of the superior/inferior RNFL using the RNFL Temporal-Superior-Nasal-Inferior-Temporal (TSNIT) curve of the Cirrus HD-OCT. The peak locations appeared to be 1 of the 256 points that ranged from 0 to 255 provided by the Cirrus HD-OCT algorithm. The peak location obtained from the TSNIT curve was translated to units of degrees by multiplying 360/256. For example, the superior peak location of 49 in the TSNIT curve was translated to 68.91° (49 × 360/256). This means that the thickest superior RNFL was located at a point 68.91° away from the temporal horizontal meridian. In the same manner, the inferior peak location was translated to units of degrees.

In addition, we measured the deviated angle of the fovea-disc center axis from the horizontal midline to the line connecting the fovea and the optic disc center on each OCT image to differentiate between cyclotorsion and optic disc torsion. After considering cyclotorsion components, we redefined the calculated angle between the horizontal line (fovea-disc center) and superior peak location by a clockwise rotation, defined as the angle alpha, and the angle between the horizontal line (fovea-disc center) and inferior peak location by a counterclockwise rotation, defined as the angle beta.

Statistical Analysis

The interobserver reproducibility of the measurements of the index of tilt, torsion degree, was evaluated by calculating the intraclass correlation coefficients. All eyes were divided into three groups (inferotemporal torsion, supranasal torsion, and nontorsion groups), according to the direction of torsion. The baseline characteristics, the mean GCIPL thickness, and RNFL thickness among the groups were compared using ANOVA with post hoc Bonferroni tests. The relationship between RNFL and GCIPL thickness and the torsion degree were evaluated by linear regression analysis. The superior and inferior peak location of the RNFL among the groups was compared using ANOVA. In addition, analysis of covariance was used for the multivariate model, including spherical equivalent treated as covariate. Statistical analyses were performed using SPSS version 18.0 (SPSS, Inc., Chicago, IL). A P value less than 0.05 was considered significant.

Results

Subjects

A total of 208 eyes, 94 randomly selected eyes of 94 subjects with optic disc torsion and 114 randomly selected eyes of 114 optic disc nontorsion subjects were analyzed. The eyes with optic disc torsion were divided further into two groups according to the direction of optic disc torsion. Finally, the inferotemporal optic disc torsion ($n = 32$), supranasal optic disc torsion ($n = 62$), and optic disc nontorsion ($n = 114$) groups were assigned. Excellent interobserver reproducibility in the measurement of the index of tilt and torsion degree was observed (intraclass correlation coefficient = 0.965 and 0.977, respectively).

Table 1 lists the baseline characteristics of the optic disc torsion group and optic disc nontorsion group. No significant differences were observed between the groups in terms of age, sex ratio, spherical equivalent, axial length, anterior chamber depth, index of tilt and ratio of the eyes with tilted disc (index of tilt ≥ 0.75), ratio of the eyes with beta peripapillary atrophy, mean IOP, and central corneal thickness. All participants showed a normal visual field and their mean deviation and pattern SD scores were similar. On the other hand, situs inversus was observed much more frequently in the optic disc torsion group ($P < 0.001$).

Table 2 lists the OCT RNFL, GCIPL, total retinal thickness, and ONH parameters in the subjects divided by the presence of optic disc torsion. No significant difference in the parameters was observed between the groups.

OCT Measurements According to Torsion Direction

The optic disc torsion group was divided further into the inferotemporal torsion and supranasal torsion groups according the direction of optic disc torsion. Table 3 presents their characteristics. The baseline demographics and ocular characteristics of the groups, including optic disc nontorsion group,

Table 2. Comparison of the Spectral Domain OCT Parameters According to the Presence of Disc Torsion

	Optic Disc Torsion, $n = 94$	Optic Disc Nontorsion, $n = 114$	*P* Value*	*P* Value†
RNFL parameters				
Temporal RNFL thickness, μm	69.69 ± 13.59	68.25 ± 11.47	0.406	0.434
Superior RNFL thickness, μm	119.98 ± 13.46	121.05 ± 15.65	0.601	0.635
Nasal RNFL thickness, μm	70.67 ± 10.84	69.79 ± 11.77	0.578	0.468
Inferior RNFL thickness, μm	122.80 ± 15.41	122.43 ± 16.04	0.867	0.738
Average RNFL thickness, μm	95.76 ± 7.96	95.39 ± 9.63	0.772	0.669
GCIPL parameters				
Superotemporal thickness, μm	81.69 ± 5.91	80.29 ± 6.56	0.110	0.112
Superior thickness, μm	82.71 ± 6.43	81.88 ± 7.58	0.398	0.408
Supranasal thickness, μm	83.49 ± 6.78	83.45 ± 7.51	0.967	0.967
Inferonasal thickness, μm	81.22 ± 7.04	81.31 ± 7.06	0.932	0.933
Inferior thickness, μm	79.46 ± 6.79	78.96 ± 6.15	0.584	0.577
Inferotemporal thickness, μm	82.27 ± 6.39	81.27 ± 5.98	0.249	0.239
Minimal GCIPL thickness, μm	77.96 ± 8.59	77.82 ± 8.63	0.912	0.892
Average GCIPL thickness, μm	81.88 ± 5.62	81.14 ± 6.35	0.378	0.376
Total retinal thickness parameters				
Central subfield thickness, μm	247.51 ± 21.91	245.28 ± 20.10	0.444	0.430
Cube volume, mm^3	9.98 ± 0.47	9.92 ± 0.43	0.365	0.346
Cube average thickness, μm	279.37 ± 12.99	277.54 ± 12.06	0.292	0.275
ONH parameters				
Rim area, mm^2	1.19 ± 0.18	1.18 ± 0.23	0.808	0.872
Optic disc area, mm^2	2.17 ± 0.55	2.10 ± 0.42	0.264	0.264
Average cup-to-disc ratio	0.64 ± 0.12	0.63 ± 0.12	0.826	0.767
Vertical cup-to-disc ratio	0.59 ± 0.12	0.59 ± 0.13	0.907	0.808
Cup volume, mm^3	0.36 ± 0.29	0.33 ± 0.22	0.313	0.292

Data are given as mean ± SD.
* Value for comparing optic disc torsion and optic disc nontorsion.
† Value for multivariate analysis after controlling for spherical equivalent.

were similar, except torsion degree and percentage of presence of the situs inversus. Table 4 lists the OCT parameters according to the direction of the optic disc torsion. The temporal RNFL segment was the only significantly different parameter according the torsion direction, which tended to be thicker in the inferotemporal torsion group than the other groups. Note that all subsectors of the GCIPL parameters were similar according the torsion direction. In the total retinal thickness and ONH parameters, all parameters were similar in the groups (all $P > 0.05$). Multivariate modeling controlling for spherical equivalent also produced similar results (Table 4).

Relationship Between Optic Disc Torsion Degree and Temporal RNFL Thickness

The temporal quadrant of RNFL thickness was thicker in inferotemporal torsion and linear regression revealed a significant correlation between the torsion degree and

Table 3. Comparison of the Characteristics Divided by Optic Disc Torsion Direction

Characteristics	Inferotemporal Torsion, $n = 32$	Supranasal Torsion, $n = 62$	Nontorsion, $n = 114$	*P* Value‡
Age, y	44.78 ± 15.76	50.10 ± 12.15	50.59 ± 13.02	0.086
Female, *n*, %*	15, 46.9	31, 50.0	45, 39.5	0.376
Spherical equivalent error, D	−1.08 ± 1.91	−0.98 ± 1.98	−0.96 ± 1.95	0.953
Axial length, mm	24.16 ± 0.80	23.71 ± 1.12	23.09 ± 4.05	0.604
Anterior chamber depth, mm	3.20 ± 0.42	3.02 ± 0.52	3.12 ± 0.40	0.582
Torsion degree†	31.08 ± 21.08	34.48 ± 17.27	7.32 ± 3.98	<0.001
Index of tilt	0.88 ± 0.08	0.88 ± 0.07	0.88 ± 0.07	0.867
Tilted disc, %*	2, 6.3	3, 4.8	4, 3.5	0.717
Situs inversus, %*	14, 43.8	25, 40.3	14, 12.3	<0.001
Beta- peripapillary atrophy, %*	10, 31.3	19, 30.6	31, 27.2	0.844
Mean IOP, mm Hg	13.58 ± 2.92	14.21 ± 2.82	14.63 ± 3.28	0.236
Central corneal thickness, μm	531.15 ± 25.95	553.85 ± 37.44	555.79 ± 38.62	0.109
Mean deviation, dB	−1.27 ± 1.58	−1.32 ± 1.77	−1.40 ± 1.69	0.932
Pattern standard deviation, dB	1.96 ± 1.40	2.06 ± 1.29	1.73 ± 0.73	0.220

Data are given as mean ± SD.
* Nonparametric values were compared by chi-square test.
† An absolute value was used in this analysis.
‡ Value for ANOVA tests comparing among inferotemporal optic disc torsion, supranasal optic torsion, and nontorsion groups.

Table 4. Comparison of the Characteristics Divided by Optic Disc Torsion Direction

	Inferotemporal Torsion, $n = 32$	Supranasal Torsion, $n = 62$	Nontorsion, $n = 114$	*P* Value*	*P* Value†
RNFL parameters					
Temporal RNFL thickness, μm	74.56 ± 15.97	67.18 ± 11.54	68.25 ± 11.47	0.017	0.018
Superior RNFL thickness, μm	116.16 ± 11.98	121.95 ± 13.84	121.05 ± 15.65	0.168	0.173
Nasal RNFL thickness, μm	69.19 ± 9.17	71.44 ± 11.61	69.79 ± 11.77	0.568	0.523
Inferior RNFL thickness, μm	123.06 ± 14.71	122.66 ± 15.88	122.43 ± 16.04	0.979	0.931
Average RNFL thickness, μm	95.72 ± 7.04	95.77 ± 8.45	95.39 ± 9.63	0.959	0.912
GCIPL parameters					
Superotemporal thickness, μm	80.91 ± 6.78	82.10 ± 5.42	80.29 ± 6.56	0.192	0.199
Superior thickness, μm	81.38 ± 6.98	83.40 ± 6.07	81.88 ± 7.58	0.295	0.310
Supranasal thickness, μm	83.13 ± 5.95	83.68 ± 7.21	83.45 ± 7.51	0.939	0.946
Inferonasal thickness, μm	79.78 ± 6.26	81.97 ± 7.35	81.31 ± 7.06	0.361	0.376
Inferior thickness, μm	78.50 ± 5.00	79.95 ± 7.54	78.96 ± 6.15	0.505	0.518
Inferotemporal thickness, μm	81.88 ± 7.07	82.47 ± 6.06	81.27 ± 5.98	0.467	0.459
Minimal GCIPL thickness, μm	77.13 ± 8.35	78.39 ± 8.74	77.82 ± 8.63	0.793	0.798
Average GCIPL thickness, μm	80.94 ± 4.81	82.37 ± 5.97	81.14 ± 6.35	0.374	0.385
Total retinal thickness parameters					
Central subfield thickness, μm	247.28 ± 25.07	247.63 ± 20.14	245.28 ± 20.10	0.745	0.729
Cube volume, mm^3	9.91 ± 0.44	10.01 ± 0.48	9.92 ± 0.43	0.393	0.389
Cube average thickness, μm	277.84 ± 11.95	280.16 ± 13.53	277.54 ± 12.06	0.400	0.391
ONH parameters					
Rim area, mm^2	1.21 ± 0.17	1.17 ± 0.19	1.18 ± 0.23	0.676	0.662
Optic disc area, mm^2	2.16 ± 0.46	2.18 ± 0.60	2.10 ± 0.42	0.531	0.534
Average cup-to-disc ratio	0.64 ± 0.10	0.64 ± 0.14	0.63 ± 0.12	0.973	0.951
Vertical cup-to-disc ratio	0.60 ± 0.10	0.59 ± 0.13	0.59 ± 0.13	0.894	0.860
Cup volume, mm^3	0.32 ± 0.20	0.38 ± 0.32	0.33 ± 0.22	0.276	0.272

Data are given as mean ± SD.
* Value for ANOVA tests comparing inferotemporal optic disc torsion, supranasal optic torsion, and nontorsion groups.
† Value for multivariate analysis after controlling for spherical equivalent.

temporal RNFL thickness (correlation coefficient = –0.075, $P = 0.025$), whereas the other RNFL quadrants and all subsectors of the GCIPL had no significant correlation with the torsion degree (Fig. 1).

Superior and Inferior Peak Locations of the RNFL According Torsion Direction

Average deviated angle of the fovea-disc center axis was –8.17° (SD ±3.56°; range, –19.96°–2.77°) in the 208 eyes. After considering the fovea-disc center axis, a smaller angle alpha, indicating a more temporalized superior RNFL peak point of the TSNIT curve, was observed in the eyes of the inferotemporal group compared with the supranasal torsion group and nontorsion group ($P < 0.001$ and $P = 0.005$, respectively), and this was significantly different among groups ($P < 0.001$). On the other hand, the angle beta, inferior RNFL peak point of the TSNIT curve, was similar in the groups ($P = 0.239$; Fig. 2).

Discussion

In this study, we investigated the characteristics of the RNFL and the GCIPL parameters according to the direction of optic disc torsion. The optic disc cube protocol of Cirrus HD-OCT constantly measures the RNFL thickness along a circular path around the optic disc. Therefore, individual optic disc variability, including optic disc torsion, can affect circumpapillary RNFL measurements, segmentation, and even diagnostic ability in glaucoma. GCIPL measurements, however, scan the macular area and obtain relatively constant measurements, irrespective of the variability of optic disc compared with circumpapillary RNFL measurements.

Our results have reported that the temporal segment thickness of the RNFL scan had a tendency to measure thicker within the subjects who had inferotemporal optic disc torsion. Recently, Hwang et al.[21] reported similar distribution patterns of the RNFL in eyes with counterclockwise rotation, which is regarded as a synonym of the inferotemporal optic disc torsion, within eyes with myopic optic disc tilt.

In the framework of the geometric relationship between the optic disc and fovea, the fovea is 2° to 6° below the center of the optic disc[13] and approximately 4 mm temporal and 0.8 mm inferior to the center of the horizontal plane of the optic disc.[22] This suggests that different trajectories between the superotemporal and inferotemporal RNFL bundles could contribute to the difference in the RNFL distribution. A previous study investigating angle alpha and angle beta, which were determined by the peak location of RNFL by OCT imaging, reported a 4° to 5° more vertically angle alpha than angle beta in the healthy controls.[20,21] In our study, angle alpha and angle beta were defined considering fovea-disc center angle. The inferotemporal disc torsion group, nontorsion group, and supranasal disc torsion group all showed smaller angle beta than angle alpha, consistent with a previous study.

Our results showed that the temporalized superior peak was observed in the inferotemporal optic disc torsion group. This could be explained at least in part by the spatial relation of the fovea-disc center axis, which generally prefers a location inferior to the optic disc. We propose a hypothesis that the amount of axonal distortion could be different between superior and inferior bundles. Due to the spatial relationship between optic disc and macular center, inferotemporally

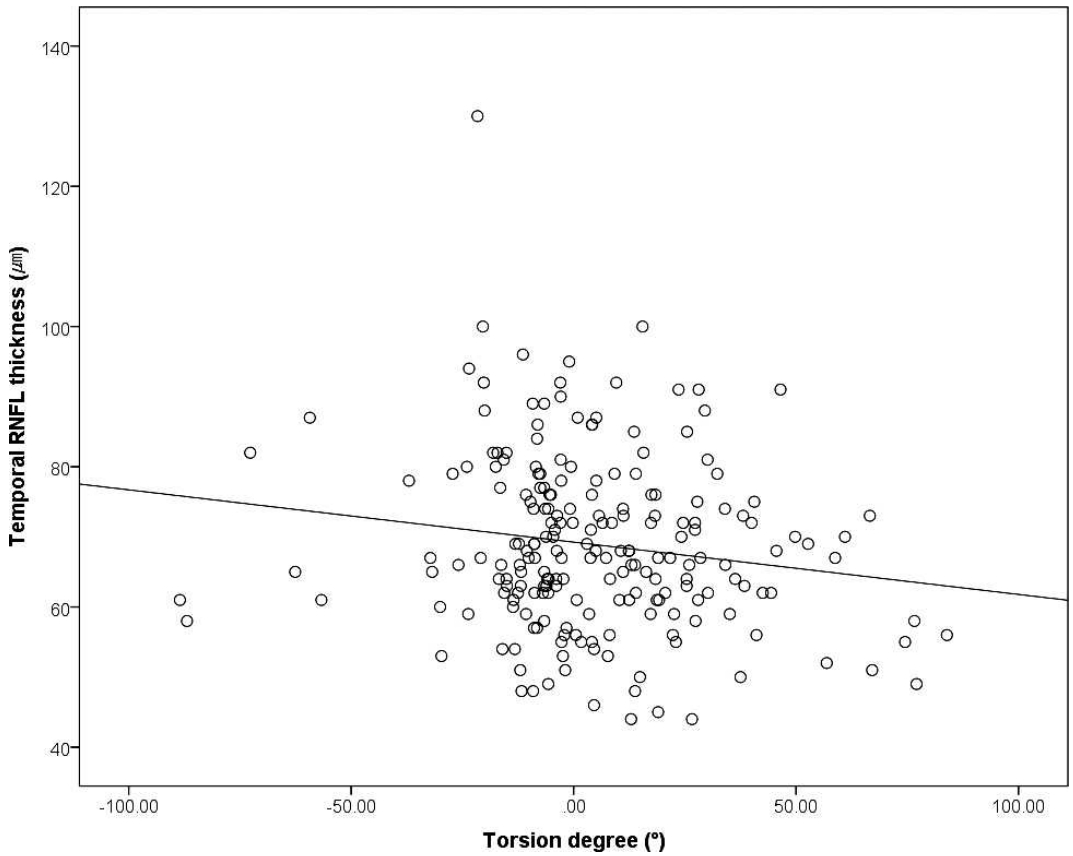

FIGURE 1. Scatterplots showing the relationship between the torsion degree and temporal RNFL thickness measured by spectral domain OCT (slope = –0.075, $P = 0.025$).

projecting RNFL fibers could be a more horizontal projection to the horizontal raphe, whereas the superotemporal RNFL is projected a bit more vertically. As mentioned previously, the optic disc cube protocol of Cirrus HD-OCT constantly scans a 1.73-mm radius around the optic disc. In Figure 3, the same distance of torsion to the opposite vector would be exaggerated to a larger distance of torsion at a 3.46-mm diameter around the normal average of 1.50- to 1.90-mm-diameter optic disc[23–27] when it projects more vertically, particularly in the superotemporal peak location of the inferotemporal optic disc torsion. More apparent temporal shift of the superior peak RNFL in eyes with inferotemporal torsion could have potential to increase the temporal quadrant RNFL thickness. However, this explanation is confined to eyes with equal deviation angle of fovea-disc center axis from horizontal midline. Further investigations are needed to better characterize structural change of optic disc torsion by use of three-dimensional imaging technology.

Although temporal quadrant RNFL thickness tends to be least affected in glaucoma, temporal quadrant RNFL thickness and distributional changes attributable to optic disc torsion should be considered. Thickening of the temporal RNFL with temporal shifting of the superior peak in eyes with inferotemporal optic disc torsion can lead to interpretation errors because OCT provides sectional analysis of the peripapillary RNFL thickness based on the normative database. The effect is small but clinically relevant in the interpretation of circumpapillary RNFL measurements. In this situation, the GCA algorithm would be helpful in differentiating eyes with optic disc torsion.

Recently, Chauhan et al.[28] introduced methods of RNFL segmentation by adjusting the fovea–Bruch's membrane opening axis setting to "0 degrees." They used Spectralis SD-OCT (Heidelberg Engineering, Heidelberg, Germany) anatomic systemic position software, which was able to offer compensatory anatomic variations between fovea and the optic disc position using the fovea–Bruch's membrane opening axis.[28–31] These comprehensive analyses of the optic nerve head might be beneficial for the accurate assessment of glaucoma, especially in cases accompanied by optic disc torsion.

This study had several limitations. First, the sample size was relatively small. In particular, the sample size of each subgroup according to the direction of optic disc torsion was too small to evaluate the difference in the characteristics thoroughly according to each subgroup. Therefore, further study with more patients will be needed. Second, the subjects in this study were identified in a referral clinic–based practice and not via population-based screening. Therefore, they cannot represent the characteristics of individuals in the general population. Future population-based surveys to evaluate the significance and characteristics of optic disc torsion will be needed to confirm these findings. Third, the average axial length of the inferotemporal optic disc torsion group was longer than the other groups, even though there was no significant difference in refraction and axial length according to torsion direction. Previous studies reported that as the axial length becomes longer, the eyeball would be stretched, the retina could be dragged toward the temporal horizon, and the RNFL layers would be compressed against the bundles originating from the opposite hemisphere at the horizontal raphe.[20,21,32–34] The myopia-related RNFL temporalization could not be excluded as one possible reason that might contribute to our results.

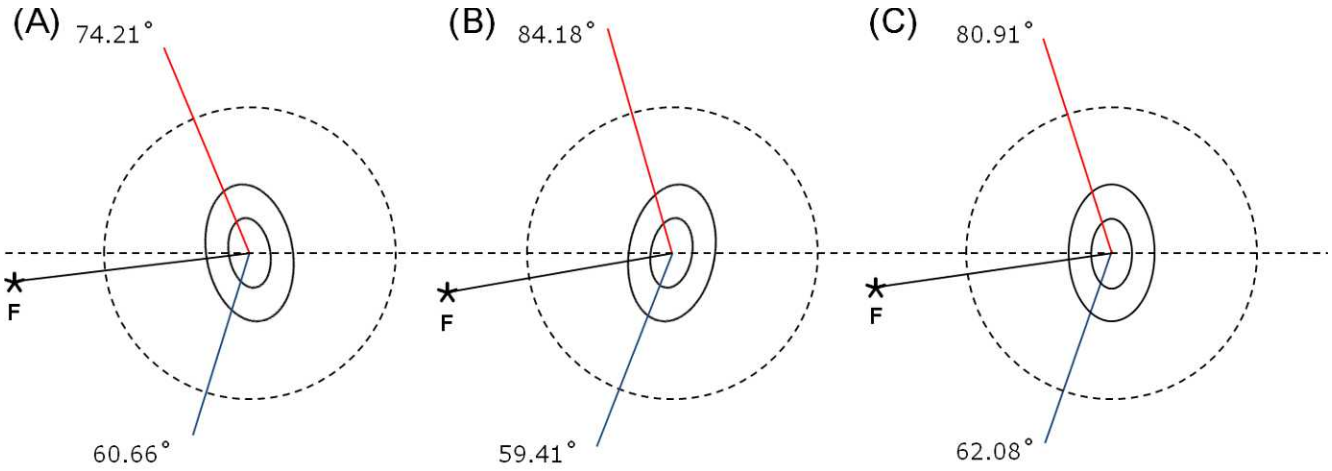

	Inferotemporal torsion	Supranasal torsion	Non-torsion	P†
Angle Alpha (°)	74.21 ± 10.49	84.18 ± 10.61	80.91 ± 9.70	<0.001
Angle Beta (°)	60.66 ± 9.48	59.41 ± 11.42	62.08 ± 9.41	0.239
Deviated angle of Fovea-Disc center axis (°)*	-6.14 ± 2.20	-9.83 ± 3.76	-7.83 ± 3.38	<0.001

*Negative value for the angle which the fovea is below the horizontal line; positive value for the angle which the fovea is above the horizontal line.
†Value for ANOVA tests.

Figure 2. Illustration of the peak locations of the RNFL presented by the alpha and beta angles according torsion direction. The *black dashed rings* indicate the 1.73 radius-peripapillary circles, which were determined for the Cirrus HD-OCT RNFL thickness profiles. F indicates fovea; therefore, *solid black lines* indicate each fovea-disc center axis deviation. The *red* and *blue solid lines* indicate the mean value of angle alpha and beta, respectively. Angle alpha was an angle between the horizontal line (fovea-disc center) and superior peak location by a clockwise rotation, and angle beta was an angle between the horizontal line (fovea-disc center) and inferior peak location by a counterclockwise rotation. (**A**) In the inferotemporal optic disc torsion group. (**B**) In the optic disc nontorsion group. (**C**) In the supranasal optic disc torsion group.

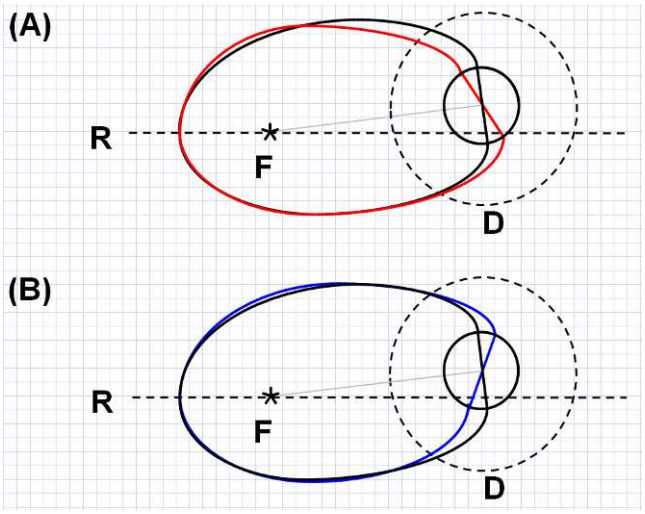

Figure 3. Illustrations of the trajectories of the peak locations of the RNFL according to torsion direction with a reflecting geometric relationship between the optic disc and fovea; the fovea is located at approximately 4 mm temporal and 0.8 mm inferior to the center of the horizontal plane of the optic disc, and the *dashed circle* indicates the OCT RNFL profile 3.46 mm diameter around the normal average of the 1.80-mm-diameter optic disc. (**A**) *Red line* indicates inferotemporal torsion disc; (**B**) *blue line* indicates supranasal torsion disc. D, optic disc; F, fovea; R, horizontal raphe.

In conclusion, the direction of optic disc torsion influences the circumpapillary RNFL thickness, whereas the macular GCIPL thickness at all segments is not affected. The temporal RNFL thickness was significantly different according to the direction of disc torsion, and the inferotemporal optic torsion contained more temporally positioned superior peak locations of the RNFL and a thicker temporal RNFL than the nontorsion and supranasal-torted optic disc, whereas the GCIPL thickness at all quadrants showed a similar torsion degree.

Acknowledgments

Supported by the Basic Science Research Program through the National Research Foundation of Korea (NRF) funded by the Ministry of Science, Information and Communication Technologies (ICT), and Future Planning (Grant NRF-2013R1A1A1010814). The authors alone are responsible for the content and writing of the paper.

Disclosure: **K.H. Lee**, None; **C.Y. Kim**, None; **N.R. Kim**, None

References

1. Apple DJ, Rabb MF, Walsh PM. Congenital anomalies of the optic disc. *Surv Ophthalmol*. 1982;27:3–41.
2. Young SE, Walsh FB, Knox DL. The tilted disc syndrome. *Am J Ophthalmol*. 1976;82:16–23.
3. Stur M. Congenital tilted disc syndrome associated with parafoveal subretinal neovascularization. *Am J Ophthalmol*. 1988;105:98–99.

4. Dimitrakos SA, Safran AB. The tilted disc syndrome: differential diagnosis of chiasmatic disorders. *Ophthalmologica*. 1982; 184:30–39.
5. Vongphanit JV, Mitchell P, Wang JJ. Population prevalence of tilted optic discs and the relationship of this sign to refractive error. *Am J Ophthalmol*. 2002;133:679–685.
6. Quigley HA, Brown AE, Morrison JD, et al. The size and shape of the optic disc in normal human eyes. *Arch Ophthalmol*. 1990;108:51–57.
7. Tay E, Seah SK, Chan SP, et al. Optic disc ovality as an index of tilt and its relationship to myopia and perimetry. *Am J Ophthalmol*. 2005;139:247–252.
8. How AC, Tan GS, Chan YH, et al. Population prevalence of tilted and torted optic discs among an adult Chinese population in Singapore. *Arch Ophthalmol*. 2009;127:894–899.
9. Giuffre G. Chorioretinal degenerative changes in the tilted disc syndrome. *Int Ophthalmol*. 1991;15:1–7.
10. Jonas JB, Kling F, Grundler AE. Optic disc shape, corneal astigmatism and amblyopia. *Ophthalmology*. 1997;104:1934–1937.
11. Witmer MT, Margo CE, Drucker M. Tilted optic discs. *Surv Ophthalmol*. 2010;55:403–428.
12. Samarawickrama C, Mitchell P, Tong L, et al. Myopia-related optic disc and retinal changes in adolescent children from Singapore. *Ophthalmology*. 2011;118:2050–2057.
13. Park HY, Lee K, Park CK. Optic disc torsion direction predicts the location of glaucomatous damage in normal-tension glaucoma patients with myopia. *Ophthalmology*. 2012;119: 1844–1851.
14. Loduca AL, Zhang C, Zelkha R, et al. Thickness mapping of retinal layers by spectral-domain optical coherence tomography. *Am J Ophthalmol*. 2010;150:849–855.
15. Wang M, Hood DC, Cho JS, et al. Measurement of local retinal ganglion cell layer thickness in patients with glaucoma using frequency-domain optical coherence tomography. *Arch Ophthalmol*. 2009;127:875–881.
16. Mwanza JC, Oakley JD, Budenz DL, et al. Macular ganglion cell-inner plexiform layer: automated detection and thickness reproducibility with spectral domain-optical coherence tomography in glaucoma. *Invest Ophthalmol Vis Sci*. 2011;52: 8323–8329.
17. Ishikawa H, Stein DM, Wollstein G, et al. Macular segmentation with optical coherence tomography. *Invest Ophthalmol Vis Sci*. 2005;46:2012–2017.
18. Tan O, Li G, Lu AT, et al. Mapping of macular substructures with optical coherence tomography for glaucoma diagnosis. *Ophthalmology*. 2008;115:949–956.
19. Van Buren JM. *The Retinal Ganglion Cell Layer: A Physiological-Anatomical Correlation in Man and Primates of the Normal Topographical Anatomy of the Retinal Ganglion Cell Layer and Its Alterations With Lesions of the Visual Pathways*. Springfield, IL: Charles C. Thomas; 1963.
20. Hwang YH, Yoo CK, Kim YY. Myopic optic disc tilt and the characteristics of peripapillary retinal nerve fiber layer thickness measured by spectral-domain optical coherence tomography. *J Glaucoma*. 2012;21:260–265.
21. Hwang YH, Yoo CK, Kim YY. Characteristics of peripapillary retinal nerve fiber layer thickness in eyes with myopic optic disc tilt and rotation. *J Glaucoma*. 2012;21:394–400.
22. Yannuzzi LA. *The Retina Atlas*. 1st ed. Philadelphia, PA: Elsevier; 2010.
23. Kanski JJ, Bowling B. Glaucoma. In: Kanski JJ, Bowling B, eds. *Clinical Ophthalmology: A Systemic Approach*. 7th ed. Edinburgh: Elsevier Saunders; 2011:311–400.
24. Quingley HA, Brown AE, Morrison JD, Drance SM. The size and shape of the optic disc in normal human eyes. *Arch Opthalomol*. 1990;108:51–57.
25. Jonas JB, Gusek GC, Naumann GO. Optic disc, cup and neuroretinal rim size, configuration and correlations in normal eyes. *Invest Ophthalmol Vis Sci*. 1988;29:1151–1158.
26. Jonas JB, Gusek GC, Guggenmoos-Holzmann I, Naumann GO. Variability of the real dimensions of normal human optic discs. *Graefes Arch Clin Exp Ophthalmol*. 1988;226:332–336.
27. Kashiwagi K, Tamura M, Abe K, Kogure S, Tsukahara S. The influence of age, gender, refractive error, and optic disc size on the optic disc configuration in Japanese normal eyes. *Acta Ophthalmol Scand*. 2000;78:200–203.
28. Chauhan BC, Burgiyne CF. Perspectives; from clinical examination of the optic disc to clinical assessment of the optic nerve head: a paradigm change. *Am J Ophthalmol*. 2013;156: 218–227.
29. Reis AS, Sharpe GP, Yang H, et al. Optic disc margin anatomy in patients with glaucoma and normal controls with spectral domain optical coherence tomography. *Ophthalmology*. 2012; 119:738–747.
30. Reis AS, O'Leary N, Yang H, et al. Influence of clinically invisible, but optical coherence tomography detected, optic disc margin anatomy on neuroretinal rim evaluation. *Invest Ophthalmol Vis Sci*. 2012;53:1852–1860.
31. Chauhan BC, O'Leary N, Almobarak FA, et al. Enhanced detection of open-angle glaucoma with an anatomically accurate optical coherence tomography-derived neuroretinal rim parameter. *Ophthalmology*. 2013;120:535–543.
32. Kim MJ, Lee EJ, Kim TW. Peripapillary retinal nerve fiber layer thickness profile in subjects with myopia measured using the Stratus optical coherence tomography. *Br J Ophthalmol*. 2010;94:115–120.
33. Hong SW, Ahn MD, Kang SH, et al. Analysis of peripapillary retinal nerve fiber distribution in normal young adult. *Invest Ophthalmol Vis Sci*. 2010;51:3515–3523.
34. Kang SH, Hong SW, Im SK, et al. Effect of myopia on the thickness of the retinal nerve fiber layer measured by Cirrus HD optical coherence tomography. *Invest Ophthalmol Vis Sci*. 2010;51:4075–4083.

Investigative Ophthalmology & Visual Science